The Meteoritical Society

*Meteoritics & Planetary Science* 55, Nr 10, 2241–2255 (2020)
doi: 10.1111/maps.13571

# Hf-W chronology of a macrochondrule from the L5/6 chondrite Northwest Africa 8192

Jan L. HELLMANN*[1], Thomas S. KRUIJER[1,2], Knut METZLER[1], Markus PATZEK[1], Andreas PACK[3], Jasper BERNDT[4], and Thorsten KLEINE[1]

[1]Institut für Planetologie, University of Münster, Wilhelm-Klemm-Strasse 10,48149 Münster, Germany
[2]Nuclear & Chemical Sciences Division, Lawrence Livermore National Laboratory, 7000 East Avenue L-231, Livermore, California 94550, USA
[3]Geowissenschaftliches Zentrum, University of Göttingen, Goldschmidtstr. 1-3,37077 Göttingen, Germany
[4]Institut für Mineralogie, University of Münster, Corrensstrasse 24,48149 Münster, Germany
*Corresponding author. E-mail: jan.hellmann@uni-muenster.de

*(Received 25 February 2020; revision accepted 20 August 2020)*

**Abstract**–A large, igneous-textured, and 2 cm-sized spherical object from the L5/6 chondrite NWA 8192 was investigated for its chemical composition, petrography, O isotopic composition, and Hf-W chronology. The petrography and chemical data indicate that this object closely resembles commonly found chondrules in ordinary chondrites and is therefore classified as a "macrochondrule.* As a result of metal loss during its formation, the macrochondrule exhibits elevated Hf/W, which makes it possible to date this object using the short-lived $^{182}$Hf-$^{182}$W system. The Hf-W data provide a two-stage model age for metal–silicate fractionation of 1.4 ± 0.6 Ma after Ca-Al-rich inclusion (CAI) formation, indicating that the macrochondrule formed coevally to normal-sized chondrules from ordinary chondrites. By contrast, Hf-W data for metal from the host chondrite yield a younger model age of ~11 Ma after CAIs. This younger age agrees with Hf-W ages of other type 5–6 ordinary chondrites, and corresponds to the time of cooling below the Hf-W closure temperature during thermal metamorphism on the parent body. The Hf-W model age difference between the macrochondrule and the host metal demonstrates that the Hf-W systematics of the bulk macrochondrule were not disturbed during thermal metamorphism, and therefore, that the formation age of such objects can still be determined even in strongly metamorphosed samples. Collectively, this study illustrates that chondrule formation was not limited to mm-size objects, implying that the rarity of macrochondrules reflects either that this process was very inefficient, that subsequent nebular size-sorting decimated large chondrules, or that large precursors were rare.

## INTRODUCTION

Large igneous inclusions are rare but important components in some ordinary chondrites (e.g., Binns 1967; Prinz et al. 1988; Weisberg et al. 1988; Bridges and Hutchison 1997; Ruzicka et al. 1998, 2000, 2012, 2019; Weyrauch and Bischoff 2012). Due to their low metal content, they stand out as bright objects on meteorite cut faces, even in terrestrially altered samples (Fig. 1). They exhibit diameters of up to ~4 cm (Bridges and Hutchison 1997) and, as such, are unusually large compared to the more common chondrules, which can be up to 5 mm in size (Weisberg et al. 1988). Owing to their large size, large igneous inclusions are more resistant to thermal metamorphism on the parent body and, therefore, occur even in highly metamorphosed samples (e.g., Bridges and Hutchison 1997; Ruzicka et al. 1998). By contrast, normal-sized chondrules in type 5 and 6 chondrites are commonly overprinted by thermal metamorphism.

The origin of large igneous inclusions is debated. They have previously been interpreted as macro- or mega-chondrules (e.g., Binns 1967; Bridges and Hutchison 1997; Ruzicka et al. 1998; Weyrauch and

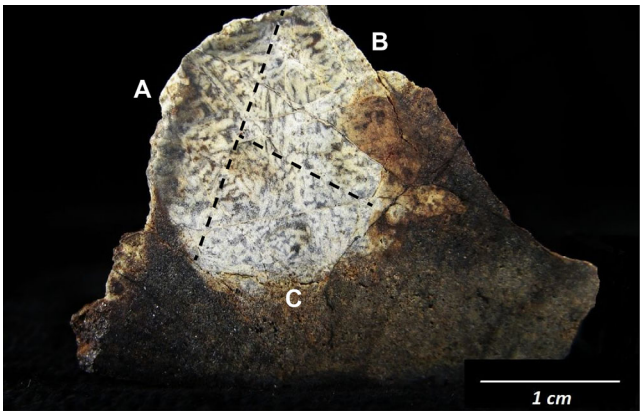


Fig. 1. Cut face of the L5/6 chondrite NWA 8192. The light object (maximum diameter of 2.1 cm) represents the investigated large igneous inclusion 8192-I1. The dashed lines indicate the locations of the subsamples A, B, and C. The host chondrite appears dark due to terrestrial weathering. (Color figure can be viewed at wileyonlinelibrary.com.)

Bischoff 2012), impact melt rocks (e.g., Bridges and Hutchison 1997; Ruzicka et al. 1998, 2000, 2019; Jamsja and Ruzicka 2010), or igneous differentiates (Kennedy et al. 1992; Sack et al. 1994; Bridges and Hutchison 1997; Ruzicka et al. 2012). Based on their chemical composition, Ruzicka et al. (2019) subdivided large igneous inclusions into four main types, including (1) vapor-fractionated inclusions; (2) unfractionated inclusions; (3) inclusions with unfractionated chemical composition, except for a strong enrichment in K; and (4) feldspar-rich inclusions. These authors proposed that vapor-fractionated inclusions have formed primarily by evaporative melting in the solar nebula and probably have a similar origin as normal chondrules. Unfractionated inclusions may have multiple origins and either formed by late impact melting of chondritic material or melted prior to thermal metamorphism and were subsequently chemically modified by open system exchange during thermal metamorphism. Unfractionated inclusions with enrichment in K are thought to have formed by impact melting of chondritic protoliths, whereas feldspar-rich inclusions may have formed by nonequilibrium shock melting and concentration of a feldspar component.

Understanding the origin of large igneous inclusions requires knowledge of their formation time. For instance, if these inclusions formed by similar processes as normal-sized chondrules, then they should have formed at about the same time, at 2–3 Ma after formation of Ca-Al-rich inclusions (CAIs; e.g., Kita et al. 2000; Rudraswami and Goswami 2007; Villeneuve et al. 2009; Pape et al. 2019). By contrast, a later formation time, after the accretion of chondrite parent bodies, would argue for an origin by impact-induced melting.

Dating the formation of large igneous inclusions has proven difficult, however, because in these objects, chronometers that are commonly used to date meteorite components (e.g., $^{26}$Al-$^{26}$Mg, $^{207}$Pb-$^{206}$Pb) are typically reset by parent body processes. By contrast, the short-lived $^{182}$Hf-$^{182}$W system (half-life = 8.9 Ma) is well suited to determine formation ages of large igneous inclusions, because their formation is associated with metal–silicate separation, and hence, fractionation of lithophile Hf from siderophile W. Thus, a model age of metal–silicate separation from the chondrite host can be calculated from the Hf-W isotope composition of a single bulk inclusion. Until now, the Hf-W system has mainly been used as a chronometer of planetary core formation (e.g., Kleine and Walker 2017), as well as to determine ages for bulk chondrites (e.g., Kleine et al. 2008; Budde et al. 2018; Archer et al. 2019; Hellmann et al. 2019) and pooled chondrule separates (Budde et al. 2016). However, with the exception of CAIs (Burkhardt et al. 2008; Kruijer et al. 2014b), no individual chondrite components have yet been dated using the Hf-W system. This reflects the low W concentrations of typical chondrite components, which currently preclude Hf-W analyses on these objects. This is not a problem for the large igneous inclusions, however, because they are of sufficient size for precise Hf-W analyses of a single inclusion.

This study is focused on a large, igneous-textured, and spherical inclusion with a diameter of about 2 cm from the L5/6 chondrite NWA 8192 (Fig. 1). To characterize this inclusion and assess its formation process, we obtained textural, chemical, and O isotopic data. Several subsamples of the inclusion were then analyzed with the Hf-W system, with the ultimate goal to constrain the formation time and origin of the inclusion and more generally to evaluate the potential of the Hf-W system to date such objects.

## ANALYTICAL METHODS

### Optical and Scanning Electron Microscopy

The texture and mineralogy of the NWA 8192 host chondrite and the large igneous inclusion (named 8192-I1) were investigated by optical and scanning electron microscopy on polished thin sections. Investigations in transmitted and reflected light were performed with a Zeiss polarizing microscope (Axiophot). A JEOL JSM-6610LV scanning electron microscope, equipped with an energy-dispersive X-ray (EDX) analyzing system (INCA, Oxford Instruments), was used to characterize the chondrule texture in detail and to obtain mineral compositions. All mineral data were checked for stoichiometry and normalized to 100 wt%. Samples and

appropriate mineral standards were measured at an acceleration voltage of 20 kV and the beam current constancy was always controlled by a Faraday cup. Standard ZAF correction procedures were applied. Mineral standards (olivine, low-Ca pyroxene, Ca-pyroxene, chromite, and plagioclase) from the L6 chondrite Leedey (Feldstein et al. 2001) were measured repeatedly to monitor the reproducibility of the energy-dispersive system.

High-resolution backscattered electron (BSE) images were used to determine the modal amounts of the main mineral phases and, additionally, phosphate, chromite, metal, and sulfide contained in the inclusion by point counting techniques. These data have also been used to calculate the bulk chemical composition of inclusion 8192-I1 by modal recombination, based on the modal amounts of the main mineral phases (olivine, low-Ca pyroxene, Ca-pyroxene, and plagioclase), their chemical composition, and their density (see Berlin et al. 2008).

### Sample Preparation and Chemical Separation of Hf and W

For Hf-W analyses, a central slice with a thickness of ~5 mm and a mass of ~1.5 g was cut out of 8192-I1 using a diamond saw and subdivided into three fragments of about 500 mg each. The three subsamples of 8192-I1 (A-C) were ultrasonicated in de-ionized $H_2O$ and ethanol and then powdered in a precleaned agate mortar. In addition, the bulk host chondrite (~500 mg) and a pure metal fraction from the host chondrite were also analyzed. For the preparation of the metal separate, ~6.6 g of the host chondrite was gradually crushed in an agate mortar and metal was separated using a hand magnet. This metal fraction was purified by grinding under ethanol and sonication in de-ionized water and ethanol.

The sample powders (8192-I1 subsamples A, B, and C and the bulk host chondrite) were dissolved in precleaned 60 mL Savillex vials at 120°C on a hotplate using 30 mL HF–$HNO_3$ (2:1). Additionally, 500 mg of a terrestrial geological reference material (BHVO-2) and a procedural blank were prepared and processed alongside the chondrite samples. The NWA 8192 metal fraction, together with a terrestrial metal standard (NIST 129c), was dissolved in 16 mL $HNO_3$–HCl–HF (10:5:1). After digestion, the samples were dried and redissolved several times and then completely dissolved in 30 mL 6 M HCl–0.06 M HF. For determination of Hf and W concentrations, 10% (8192-I1 subsamples) or 3% aliquots (metal fraction, bulk chondrite) were spiked with a mixed $^{180}Hf$-$^{183}W$ tracer for the determination of Hf and W concentrations by isotope dilution (Kleine et al. 2002, 2004). Finally, 5% aliquots of the sample solutions were used for analyses of rare earth element (REE) concentrations by ICP-MS.

For W isotope composition analyses, W was separated from the sample matrix using a two-step anion exchange chemistry as described in Kruijer et al. (2012, 2014b). The samples were dried and redissolved in 75 mL 0.5 M HCl–0.5 M HF, and were then loaded onto precleaned anion exchange columns (4 mL BioRad AG1X8, 200–400 mesh). Most of the sample matrix was washed off the column using 10 mL 0.5 M HCl–0.5 M HF, and high field strength elements, including Hf and W, were eluted in 15 mL 6 M HCl–1 M HF. After collecting the W cuts in 15 mL Savillex vials, the metal samples were repeatedly dried down at 180°C with added concentrated $HClO_4$ to remove organic compounds and to reduce W loss associated with incomplete redissolution in PFA beakers (Kruijer et al. 2012). For the 8291-I1 subsamples and the host meteorite, the dry downs were performed with $HNO_3$ and $H_2O_2$ at max. 80 °C in order to keep the W blank as low as possible (Kleine et al. 2004). The W cuts were then completely dissolved in 1 M HF, diluted to 6 mL 0.6 M HF–0.4% $H_2O_2$, and loaded onto precleaned anion exchange columns (1 mL BioRad AG1X8, 200–400 mesh). Remaining matrix elements (most notably Ti) were removed using 10 mL 1 M HCl–2% $H_2O_2$, 9 mL 8 M HCl–0.01 M HF, and 0.5 mL 6 M HCl–1 M HF, followed by elution of W using another 8.5 mL 6 M HCl–1 M HF (see Kleine et al. 2012). The W cuts were dried and repeatedly dried down with added $HNO_3$–$H_2O_2$ (silicate-rich samples) or $HNO_3$–$HClO_4$ (metal).

The spiked aliquots were dissolved in 6 M HCl, diluted to 1 M HCl–0.5 M HF, and loaded onto precleaned anion exchange columns (1 mL BioRad AG1X8, 200–400 mesh). The columns were rinsed using 1 mL 0.5 M HCl–0.5 M HF and the matrix was washed off the columns using 5 mL 1 M HF. Hafnium was eluted using 4 mL 8 M HCl–0.01 M HF, followed by 5 mL 6 M HCl–1 M HF for the elution of W. The Hf and W cuts were dried and redissolved in $HNO_3$ and $H_2O_2$ several times. Finally, they were dissolved in 0.5 mL of a 0.56 M $HNO_3$–0.24 M HF running solution. Total procedural W blanks for isotope composition measurements were 130–310 pg (8192-I1 subsamples and host chondrite) and 225 pg (metal). These blanks were negligible for the host chondrite and the metal sample, but for the 8192-I1 subsamples, blank corrections of 1–3% were necessary. Finally, blanks for the isotope dilution measurements were 8–23 pg W and 5–16 pg Hf, and were negligible for all samples.

### W Isotope Measurements

All isotope measurements were performed using a ThermoScientific Neptune Plus MC-ICP-MS at the Institut für Planetologie in Münster. Samples were introduced into the mass spectrometer using an ESI PFA nebulizer with an uptake rate of 50–60 μL $min^{-1}$ connected to a Cetac Aridus II desolvator. Using Jet sampler and X skimmer cones, total ion beam intensities of ~1.8–1.9 × $10^{-10}$ A were obtained for a 20 ppb W solution. Each measurement consisted of 60 s baseline integrations (deflected beam), followed by 100 (8192-I1 subsamples) or 200 (metal sample and host chondrite) isotope ratio measurements of 4.2 s each. Isobaric Os interferences on $^{184}W$ and $^{186}W$ were monitored on mass $^{188}Os$ and were negligible for all samples. Instrumental mass bias was corrected relative to $^{186}W/^{184}W = 0.92767$ ("6/4") or $^{186}W/^{183}W = 1.9859$ ("6/3") using the exponential law. Results are reported as ε-unit deviations (i.e., 0.01%) relative to the mean value obtained for bracketing analyses of an Alfa Aesar standard solution (see Kleine et al. 2002, 2004).

The accuracy and reproducibility of the sample analyses were assessed by measurements of a terrestrial rock standard (BHVO-2) and a metal standard (NIST 129c) that were processed together with the meteorite samples. The average $\varepsilon^{182}W$ (6/4) obtained for analyses of BHVO-2 run at ~15 ppb yielded $\varepsilon^{182}W = -0.07 \pm 0.27$ (2 SD, $n = 7$). The uncertainty of these measurements provides a good estimate for the external reproducibility of a single W isotope measurement. For the measurements of the 8192-I1 subsamples, the external reproducibility of the BHVO-2 measurements or the internal error of the 8192-I1 measurements was adopted, whichever is larger. The host meteorite was measured at ~30 ppb W and the reported external uncertainty is based on the reproducibility of ±0.10 (2 SD) obtained for multiple measurements of BHVO-2 performed in an earlier study (Kruijer et al. 2014b). For metal samples, results are reported as the mean of quintuple 200 cycle measurements with their corresponding 95% confidence intervals. Quintuple measurements of NIST 129c yielded an $\varepsilon^{182}W$ (6/4) of $0.04 \pm 0.05$ (95% confidence), demonstrating the accuracy of the W isotope analyses. Finally, the uncertainties of the Hf and W isotope dilution measurements (2σ) were estimated from the uncertainties on the isotope ratio measurements (2 SD) and from blank corrections (<0.4%), resulting in uncertainties on $^{180}Hf/^{184}W$ ratios of <0.6%.

### Rare Earth Element Analyses

REE concentrations were determined using a ThermoScientific X-series II ICP-MS at the Institut für Planetologie in Münster. A calibration curve was determined by measuring different dilutions of the geological reference material BHVO-2. A digested aliquot of Allende MS-A (an ~100 g powder prepared from a single slice of Allende) and an in-house REE standard (REE2013B) were measured as unknown secondary standards. Indium was added to standard and sample solutions for correction of instrumental drift during the measurements. Acid blanks were measured prior to standard and sample solutions and subtracted from the intensities of standards and sample measurements.

The REE concentrations of 8192-I1 and the host chondrite were also measured using LA-ICP-MS by traversing the areas of interest and integrating the obtained signal. Sample ablation was carried out with a pulsed 193 nm ArF excimer laser (Analyte G2, Photon Machines). A repetition rate of 10 Hz and an energy of ~3–4 J $cm^{-2}$ were used throughout the session. Elemental analyses were carried out with a ThermoScientific Element 2 SF-ICP-MS. Before analyses, the system was tuned using the NIST 612 reference material glass by measuring $^{139}La$, $^{232}Th$, and $^{232}Th^{16}O$ to obtain stable signals and optimal sensitivity, as well as low oxide rates ($^{232}Th^{16}O/^{232}Th < 0.1\%$) during the ablation. The REEs were analyzed using the NIST 612 glass as an external standard and $^{43}Ca$ as the internal standard. Concentrations of measured elements were calculated using the Glitter software (Van Actherbergh et al. 2001; Griffin 2008). Standard reference glasses BCR2-G, NIST 610, GSE1-G, and GSD1-G were analyzed as monitors for precision and accuracy. The results obtained for these reference glasses generally match the published range of concentrations given in the GeoReM database (version 23; Jochum et al. 2005).

### Oxygen Isotope Analyses

A small aliquot of the sample powder from the center of inclusion 8192-I1 was used for O isotopic analysis. Prior to measurement, the magnetic components were extracted by a weak hand magnet. This procedure concentrates the O-bearing minerals and has the positive side effect of co-extracting terrestrial oxidation products that usually adhere to metal grains.

A representative aliquot of about 1 mg was taken for infrared laser fluorination in combination with gas chromatography isotope ratio gas mass spectrometry (see Pack et al. [2016] for details). Results are reported as $\delta^{17}O$ and $\delta^{18}O$ values in ‰ (parts per thousand, relative to VSMOW). Uncertainties (1σ) were ~0.04‰ for $\delta^{17}O$, ~0.08‰ for $\delta^{18}O$, and ~0.02‰ for $\Delta^{17}O$ (Metzler and Pack 2016).

## RESULTS

### Texture and Mineral Chemistry

The L5/6 chondrite NWA 8192 has a low shock stage S2 (Meteoritical Bulletin Database 2020) and a weathering grade W3 (Meteoritical Bulletin Database 2020). As a result, more than 60% of the metal grains have been replaced by secondary alteration products (Wlotzka 1993). As a type 5/6 chondrite, NWA 8192 was thermally metamorphosed to a high degree, as is evident from its recrystallized texture with frequent triple junctions between the main mineral phases (olivine, low-Ca pyroxene Ca-pyroxene, plagioclase) and the equilibrated composition of both olivine and pyroxene (see below).

Due to its large size and bright appearance, inclusion 8192-I1 stands out in the hand specimen and contrasts strongly with the brownish color of its weathered host chondrite (Fig. 1). The strong contrast is caused by the very low amount of Fe,Ni metal in this object. The inclusion has a roundish outer shape indicating that it represents a once molten spherical object. Its texture indicates rapid cooling and crystallization during supercooling, typical for non-porphyritic chondrules in ordinary chondrites. It appears to represent the metamorphosed and recrystallized equivalent of pyroxene-bearing chondrules typically found in unequilibrated ordinary chondrites (UOCs; see Fig. 2b). The inclusion mainly consists of elongated, randomly oriented units of parallel aligned skeletal olivine crystals with interstitial plagioclase. Due to the transparency of these units, they appear as lath-shaped bright regions up to ~5 mm on a cut face (Fig. 1). Over their entire length, the parallel olivine platelets in these units show identical optical extinction under the polarizing microscope, indicating that they are part of the same skeletal crystal. These regions are frequently interrupted by more isometric pyroxene crystals and pyroxene-rich units, mostly 0.5–1 mm in size. In some instances, thin olivine lamellae are enclosed in the pyroxene crystals and pyroxene-rich units. This is shown in Fig. 2a (BSE image), where olivine and pyroxene appear light gray and dark gray, respectively. Plagioclase appears as black interstitial material between the parallel olivine platelets. Although somewhat obscured by metamorphic recrystallization, this texture indicates a co-crystallization of small skeletal olivine and more isometric pyroxene crystals, followed by the growth of large skeletal olivine. The growth of the latter was obviously hampered by the already crystallized pyroxene and pyroxene-rich units. This crystallization sequence and the resulting texture


Fig. 2. a) Backscattered electron image showing the boundary (white line) between the large igneous inclusion 8192-I1 (left) and the surrounding host chondrite NWA 8192 (right). The texture of the inclusion is characterized by parallel platelets of olivine skeletal crystals (light gray) with interstitial plagioclase (black). These elongated olivine–plagioclase units reach lengths of about 5 mm and are interspersed with tiny metal grains (white). The skeletal olivine crystals are interrupted by low-Ca pyroxene crystals (dark gray; Px) and pyroxene-dominated units of similar size and shape (white elliptic outline) with random orientations. b) Backscatter electron image showing a pyroxene-bearing chondrule with skeletal olivine from the unequilibrated LL3 chondrite NWA 5206 for comparison to the macrochondrule 8192-I1 studied here.

are similar to those found for non-porphyritic chondrules in UOCs (Fig. 2b).

This mean composition of plagioclase ($An_{10.9}Or_{5.6}$; Table 1) is indistinguishable from that in the host meteorite. It probably did not crystallize directly from the melt but replaced earlier formed mesostasis in the course of thermal metamorphism. The mean compositions of olivine ($Fa_{24.9}$) and low-Ca pyroxene in the inclusion ($Fs_{20.8}Wo_{1.7}$) are also indistinguishable

Table 1. Modal and chemical compositions of the investigated large igneous inclusion and its main mineral phases (wt%).

| | Olivine | Low-Ca pyroxene | Ca-Pyroxene | Plagioclase | Phosphate | Chromite | Metal | Sulfide | Bulk inclusion[a] |
|---|---|---|---|---|---|---|---|---|---|
| Vol% | 33.1 | 6.6 | 7.3 | 50.6 | 1.3 | 0.7 | 0.3 | 0.1 | |
| Density[b] | 3.55 | 3.37 | 3.40 | 2.64 | 2.95 | 4.5 | 8.00 | 4.61 | 3.05 |
| $SiO_2$ | 38.2 | 55.4 | 53.1 | 64.7 | n.d. | 0.9 | | | 50.9 |
| $TiO_2$ | n.d. | 0.2 | 0.8 | 0.1 | n.d. | 5.0 | | | 0.2 |
| $Al_2O_3$ | n.d. | 0.1 | 0.5 | 21.6 | n.d. | 5.3 | | | 9.5 |
| $Cr_2O_3$ | 0.1 | 0.1 | 1.2 | n.d. | 0.1 | 53.5 | | | 0.7 |
| FeO | 22.7 | 13.9 | 4.9 | 0.5 | 0.5 | 30.6 | | | 10.6 |
| MnO | 0.4 | 0.5 | 0.2 | n.d. | n.d. | 0.8 | | | 0.2 |
| MgO | 38.4 | 28.9 | 16.3 | 0.1 | 3.3 | 3.3 | | | 18.2 |
| CaO | 0.1 | 0.9 | 22.4 | 2.3 | 46.6 | 0.2 | | | 3.5 |
| $Na_2O$ | 0.1 | 0.1 | 0.7 | 9.7 | 2.8 | 0.2 | | | 4.3 |
| $K_2O$ | n.d. | n.d. | n.d. | 1.0 | n.d. | 0.1 | | | 0.4 |
| $P_2O_5$ | n.d. | n.d. | n.d. | 0.1 | 46.7 | 0.1 | | | 0.6 |
| S | | | | | | | n.d. | 51.0 | 0.1 |
| Fe | | | | | | | 86.0 | 49.0 | 0.8 |
| Ni | | | | | | | 14.0 | n.d. | 0.1 |
| | $Fa_{24.9}$ | $Fs_{20.8}Wo_{1.7}$ | $Fs_{7.8}Wo_{45.8}$ | $An_{10.9}Or_{5.6}$ | | | | | |

[a]Calculated by chemical recombination based on modal abundances of the mineral phases.
[b]Mineral densities calculated from values given in Engineering ToolBox (2001; g $cm^{-3}$).

from those of the host meteorite (Meteoritical Bulletin Database 2020), indicating a high degree of thermal overprint. Ca-rich pyroxene ($Fs_{7.8}Wo_{45.8}$) occurs in small amounts (~7 vol%), mostly in close association with low-Ca pyroxene.

Metal occurs as tiny grains (typical sizes 10–50 μm) mainly in the olivine–plagioclase units and exhibits mean Ni contents of 14 wt% (5–21 wt%; $n = 8$). Compared to the metal in the host chondrite, these grains are much better preserved and show only very thin rinds of terrestrial weathering products. The phosphate minerals merrillite and apatite occur as elongated grains and show a very inhomogeneous distribution; occasionally apatite is replaced by Cl-apatite. Further accessory minerals are chromite <50 μm, chromium spinel (atomic Cr/[Cr + Al] = 0.87; Mg/[Mg + Fe] = 0.14; $TiO_2$ = 4.3 wt%), Mg-bearing ilmenite, and troilite. The modal abundances of all major minerals of the inclusion together with phosphate, chromite, metal, and sulfide are given in Table 1.

## Hf-W Systematics

The Hf-W data for the three 8192-I1 subsamples, a bulk sample of NWA 8192, and the NWA 8192 metal fraction are reported in Table 2. The 8192-I1 subsamples have uniformly low and subchondritic W concentrations of about 20 ppb. The Hf concentrations are more variable among the subsamples (493–582 ppb), but higher than those of any bulk chondrite. As a result, all 8192-I1 subsamples exhibit elevated $^{180}Hf/^{184}W$ ratios of between ~26 and ~33. Consistent with this, all three 8192-I1 samples have highly radiogenic $\varepsilon^{182}W$ values of ~28.

Two of the subsamples exhibit slightly negative $\varepsilon^{183}W$, which most likely is attributable to a mass-independent isotope fractionation introduced during sample preparation (Willbold et al. 2011; Kruijer et al. 2012; Cook and Schönbächler 2016). This effect has been observed in numerous earlier W isotope studies and most likely results from preferential loss of $^{183}W$ during W purification (e.g., Willbold et al. 2011; Kruijer et al. 2014a, 2014b; Budde et al. 2015, 2016). By contrast, the positive $\varepsilon^{183}W$ for subsample 8192-I1-A cannot be due to this effect, but most likely is due to an organic interference, which occasionally occurs during the analysis of samples with low W abundances (Kleine et al. 2008). We note that these effects on $^{183}W$ are inconsequential for $\varepsilon^{182}W$ (6/4), which will be used throughout this study.

The bulk sample of NWA 8192 has a $^{180}Hf/^{184}W$ ratio of 1.46 ± 0.01 and $\varepsilon^{182}W$ of –1.86 ± 0.12, which are typical values for L chondrites (Hellmann et al. 2019) and which are also similar to those of carbonaceous chondrites (e.g., Allende CV3; $^{180}Hf/^{184}W = 1.35 \pm 0.03$ and $\varepsilon^{182}W = -1.97 \pm 0.04$; Kruijer et al. 2014b). The metal fraction of the host chondrite has $^{180}Hf/^{184}W < 0.03$, demonstrating that a relatively pure metal separate was obtained. The metal

Table 2. Hf-W data for the macrochondrule, the host meteorite NWA 8192, and its metal fraction.

| Sample ID | | Weight (mg) | Hf (ppb) | W (ppb) | $^{180}Hf/^{184}W$ (±2σ) | Cycles | *N* | $\varepsilon^{182}W$ (6/3) (±2σ)* | $\varepsilon^{182}W$ (6/4) (±2σ)* | $\varepsilon^{183}W$ (6/4) (±2σ)* | $\varepsilon^{184}W$ (6/3) (±2σ)* |
|---|---|---|---|---|---|---|---|---|---|---|---|
| Macrochondrule (NWA 8192-I1) | | | | | | | | | | | |
| BK13 | A | 497 | 493 | 22.1 | 26.3 ± 0.1 | 100 | 1 | 25.2 ± 0.5 | 27.8 ± 0.5 | 1.91 ± 0.40 | −1.27 ± 0.27 |
| BK12 | B | 598 | 582 | 23.5 | 30.0 ± 0.2 | 100 | 1 | 28.8 ± 0.2 | 28.6 ± 0.2 | −0.10 ± 0.15 | 0.07 ± 0.10 |
| BK14 | C | 548 | 531 | 19.4 | 33.3 ± 0.1 | 100 | 1 | 28.0 ± 0.4 | 27.8 ± 0.4 | −0.17 ± 0.13 | 0.11 ± 0.09 |
| Weighted average (±2SD) | | 1643 | 538 | 21.7 | 30.0 ± 0.2 | | 3 | 27.5 ± 0.7 | 28.1 ± 0.7 | 0.48 ± 0.45 | −0.32 ± 0.30 |
| NWA 8192 (L5/6) | | | | | | | | | | | |
| BN07 | Bulk | | 160 | 129 | 1.46 ± 0.01 | 200 | 1 | −1.87 ± 0.13 | −11.86 ± 0.12 | 0.01 ± 0.09 | 0.00 ± 0.06 |
| AC09 | Metal (±95% conf.) | 246 | 22.6 | 1197 | 0.0223 ± 0.0001 | 200 | 5 | −2.41 ± 0.04 | −12.58 ± 0.04 | −10.12 ± 0.01 | 0.08 ± 0.01 |
| BHVO-2 | (±2SD) | | | | | 100 | 7 | −0.08 ± 0.34 | −10.07 ± 0.27 | −10.02 ± 0.16 | 0.04 ± 0.18 |
| NIST 129c | (±95% conf.) | | | | | 200 | 5 | 0.18 ± 0.04 | 0.04 ± 0.03 | −10.11 ± 0.03 | 0.07 ± 0.02 |

Internal mass bias fractionation was corrected using the exponential law by internal normalization to $^{186}W/^{183}W = 1.98594$ (6/3) or $^{186}W/^{184}W = 0.92767$ (6/4). *N* denotes number of solution replicates. *Cycles* denotes number of individual cycles (4.2 s) per measurement.

*Uncertainties for single measurements of subsamples A–C and bulk host chondrite represent the internal two standard error of the mean (2 SE). External uncertainties for W isotope measurements of the subsamples of the macrochondrule were calculated using the external reproducibility derived from the BHVO-2 analyses (±0.27, 2SD) run under the same conditions. In case the 2 SE after blank correction exceeded the 2 SD of BHVO-2, the 2 SE of the subsample was used instead. Uncertainties for metal samples are 95% confidence intervals for solution replicates ($N = 5$).

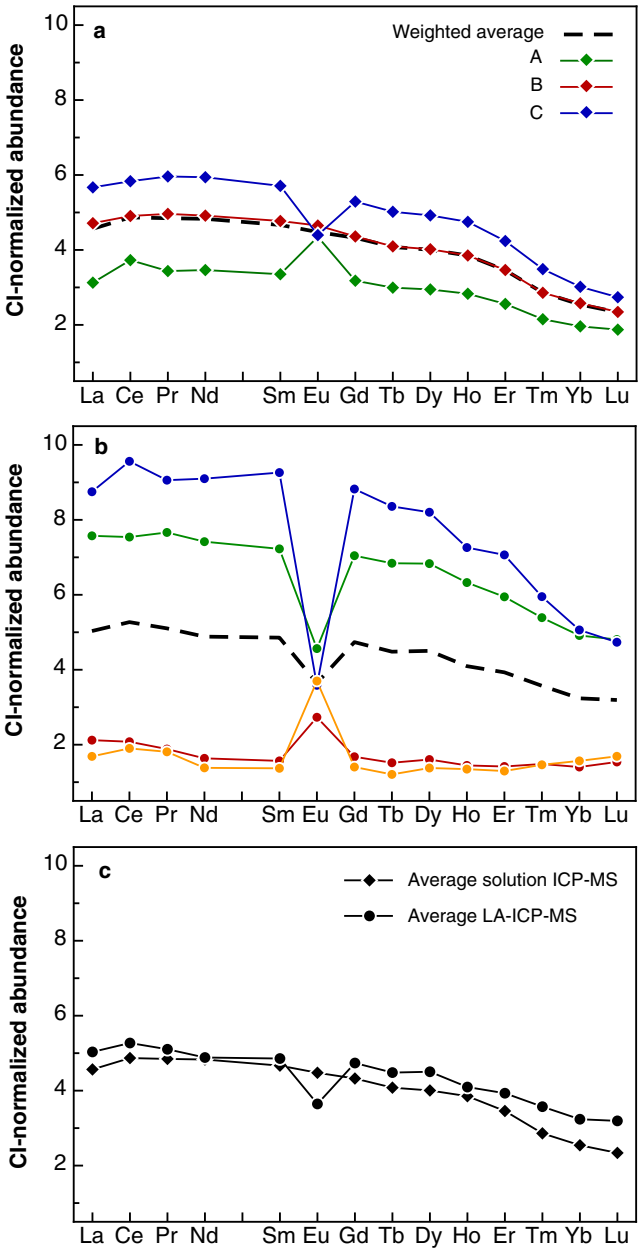


Fig. 3. a) CI-normalized REE concentrations for 8192-I1 subsamples A–C determined by solution ICP-MS. Dashed line represents the weighted average of the three subsamples. b) REE patterns of traverses across the entire inclusion obtained by laser ablation ICP-MS. Solid lines represent mean values obtained from traverses. Dashed line represents the average of the four traverses. c) Comparison of average CI-normalized REE concentrations obtained by solution ICP-MS and laser ablation ICP-MS. (Color figure can be viewed at wileyonlinelibrary.com.)

displays an $\varepsilon^{182}W$ value of $-2.58 \pm 0.04$, which is similar to values determined for metal fractions of other type 5 and 6 L and LL chondrites (Hellmann et al. 2019).

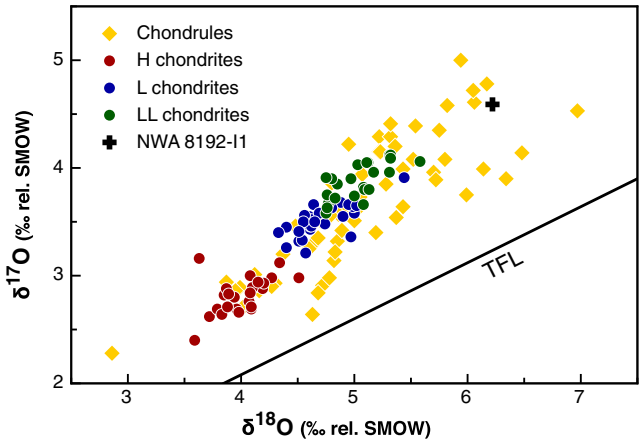


Fig. 4. Oxygen isotopic compositions of equilibrated ordinary H, L, and LL chondrites (falls) and individual chondrules from ordinary chondrites (Clayton et al. 1991). The large igneous inclusion 8192-I1 (black cross) plots away from bulk chondrites, within the field of ordinary chondrite chondrules. (Color figure can be viewed at wileyonlinelibrary.com.)

## Rare Earth Elements

Rare earth element abundances of the three 8192-I1 samples display significant enrichments relative to CI chondrites (Pourmand et al. 2012), and enrichments of the light over the heavy REEs with an La/Lu ratio of ~1.95 (Fig. 3). The three 8192-I1 subsamples have slightly different REE patterns, indicating a heterogeneous distribution of the REEs within the inclusion. For instance, whereas 8192-I1-B lacks an Eu anomaly, 8192-I1-A has a positive Eu and 8192-I1-C a complementary negative Eu anomaly. A weighted average of all three subsamples results in an REE pattern without an Eu anomaly that overall is very similar to the REE concentrations measured for 8192-I1-B, suggesting that this subsample best represents the composition of the bulk inclusion.

To further characterize the distribution of the REEs among the different mineral phases of 8192-I1, REE concentrations were also determined by averaging four traverses across the entire inclusion by laser ablation ICP-MS. Individual traverses display complementary REE patterns with positive and negative Eu anomalies, and different degrees of REE enrichments and fractionations. These differences most likely reflect a nugget effect resulting from the heterogeneous distribution of phosphate grains. The REEs are highly concentrated in phosphates like merrillite or apatite, with enrichment factors of several hundred times CI concentrations (Brearley and Jones 1998). Furthermore, REEs in phosphates are strongly fractionated, where heavy REEs are depleted relative to light REEs

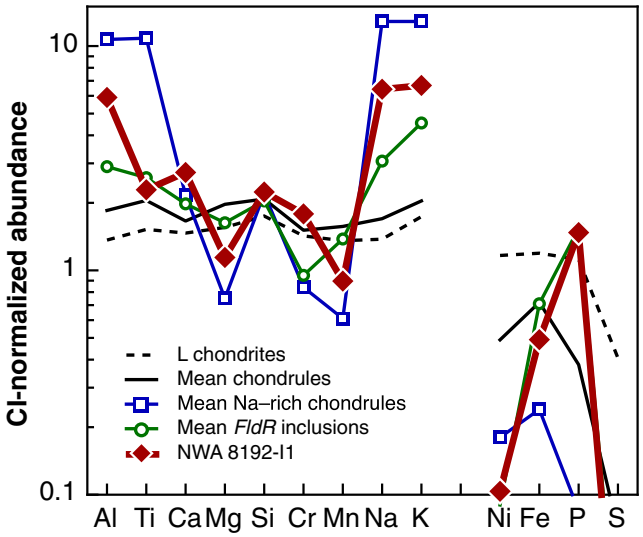


Fig. 5. CI chondrite-normalized abundances (CI abundances from Lodders 2003) for macrochondrule 8192-I1, mean bulk L chondrites (McSween and Huss 2010), and mean chondrules from ordinary chondrites (Grossman and Wasson 1983). Elements are grouped according to their 50% condensation temperature (Lodders 2003) and according to their geochemical behavior (lithophile elements on left and siderophile/chalcophile elements on right). Macrochondrule 8192-I1 is strongly enriched in Al, Na, and K and depleted in Fe, Ni, and S relative to bulk chondrites. This pattern is very similar to feldspar-rich (*FldR*) inclusions described by Ruzicka et al. (2019) and Na-rich chondrules (Ebert and Bischoff 2016). (Color figure can be viewed at wileyonlinelibrary.com.)

(Ebihara and Honda 1983). Such REE patterns have also been observed for merrillite in ordinary chondrites (Ward et al. 2017). Thus, even minute variations in the abundance of phosphate grains can result in dramatically different REE concentrations and patterns within a given sample. As such, the heterogeneous distribution of phosphate grains within the 8192-I1 inclusion can account for both the small REE differences among the 8192-I1 subsamples and the larger variations among the LA-ICP-MS traverses. In spite of these heterogeneities, the weighted average REE concentrations of the three 8192-I1 subsamples, amounting to a total sample weight of ~ 1.5 g, should provide a good estimate of the REE concentrations of the bulk inclusion.

### Oxygen Isotopes

The 8192-I1 inclusion is characterized by $\delta^{17}O = 4.59‰$ and $\delta^{18}O = 6.22‰$, corresponding to a $\Delta^{17}O$ value of 1.30‰. As shown in Fig. 4, it plots within the field of ordinary chondrite chondrules, but its $\delta^{17}O$ and $\delta^{18}O$ values are significantly higher than those of bulk ordinary chondrites (Clayton et al. 1991).

## DISCUSSION

### Origin of the Inclusion: Macrochondrule, Impact Melt, or Planetary Differentiate?

The magmatic texture and rounded shape of the 8192-I1 inclusion suggest it once was completely molten and subsequently solidified rapidly as a free-floating object in space. The chemical composition of 8192-I1 is similar to those of the feldspar-rich inclusion type defined by Ruzicka et al. (2019). This type of inclusion is strongly enriched in Al, Na, and K, and depleted in Fe, Ni, and S (Fig. 5). The depletion of Fe, Ni, and S most likely is the result of metal and sulfide segregation during formation of the inclusion. The smaller depletion of Fe compared to Ni and S may reflect formation under oxidizing conditions, resulting in abundant incorporation of FeO into silicate phases. Ruzicka et al. (2019) proposed that the feldspar-rich inclusions may have formed as partial melts of a chondritic precursor, perhaps as a result of impact melting. However, several observations are inconsistent with an impact melt origin of 8192-I1. First, impact melt rocks are thought to form mainly in the center of an impact site and, therefore, generally represent whole rock melts. Hence, with the exception of siderophile element concentrations, which are low as a result of metal segregation, most impact melt rocks exhibit the bulk chemistry of the (chondritic) target material (e.g., Metzler et al. 2011). This is not the case for 8192-I1, however (Fig. 5). For instance, $Al_2O_3$ and $SiO_2$ in the studied object are enriched by factor of ~4 and ~1.3 relative to the bulk chemistry of L chondrites (e.g., Jarosewich 2006; Metzler et al. 2011). Moreover, due to its high $SiO_2$ concentration, low-Ca pyroxene co-crystallized with olivine during cooling. This is almost never observed in ordinary chondrite impact melts, where typically olivine is the liquidus phase (e.g., Metzler et al. 2011). Second, the O isotope composition of 8192-I1 is different from that of bulk ordinary chondrites (Fig. 4), inconsistent with an origin by impact melting of known bulk ordinary chondrite material. Finally, the Hf-W model age of metal segregation (see below) indicates that 8192-I1 formed prior to or during accretion of the parent body of its chondrite host, and thus not by late impact melting on the parent body.

Another possibility is that the 8192-I1 inclusion represents a melt droplet that was excavated from the molten silicate portion of a differentiated body and accreted alongside normal-sized chondrules into the host chondrite. Consistent with this, the high Hf/W and radiogenic $\varepsilon^{182}W$ of 8192-I1 are similar to those of basaltic eucrites (Touboul et al. 2015). However, the $\Delta^{17}O$ of 1.30 of 8192-I1 is different from HED

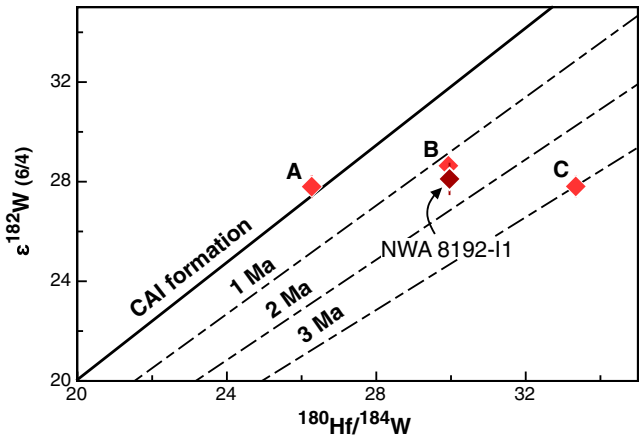


Fig. 6. Hf-W isochron diagram with reference isochrons (dashed lines) for three different times after CAI formation (1, 2, and 3 Ma; calculated using the CAI initial values from Kruijer et al., 2014b). $\varepsilon^{182}$W (6/4) is the parts per 10,000 deviation of the $^{182}$W/$^{184}$W ratio of a sample from that of the standard solution; 6/4 denotes internal normalization to $^{186}$W/$^{184}$W (see text for details). Error bars denote external uncertainties (2 SD) as described in the text. The three subsamples A, B, and C of 8192-I1 plot between the 0 and 3 Ma model isochrons, and the weighted average of the three subsamples plots between the 1 and 2 Ma isochrons. As described in the text, the weighted average composition of the three samples provides a representative estimate for the bulk composition of 8192-I1. The uniform $\varepsilon^{182}$W of the three subsamples indicates that their different Hf/W ratios were established after $^{182}$Hf extinction and most likely reflect an uneven distribution of Hf-rich phosphates among the three subsamples. (Color figure can be viewed at wile yonlinelibrary.com.)

meteorites ($\Delta^{17}$O = –0.219 ± 0.002; Wiechert et al. 2004) or other known differentiated or primitive materials, including bulk ordinary chondrites (Clayton et al. 1991; Clayton and Mayeda 1996, 1999; Newton et al. 2000; Greenwood et al. 2012). Moreover, the O isotopic composition of 8192-I1 overlaps with that of ordinary chondrite chondrules, suggesting that 8192-I1 formed from similar precursor material as the more common, normal-sized chondrules from ordinary chondrites (Fig. 4). Consistent with this, the bulk chemistry of 8192-I1 is also consistent with that of ordinary chondrite chondrules (e.g., Metzler and Pack 2016), with a strong tendency toward Na-Al-rich chondrules with their typical enrichment in refractory lithophile elements (Ebert and Bischoff 2016; Fig. 5). Finally, although 8192-I1 is extraordinarily large, objects with similar characteristics have been found previously and were classified as macrochondrules (e.g., Weisberg et al. 1988; Bridges and Hutchison 1997; Ruzicka et al. 1998; Weyrauch and Bischoff 2012). Thus, we conclude that 8192-I1 most likely formed by a similar process as ordinary chondrite chondrules, and we, therefore, classify it as a macrochondrule.

## Hf-W Model Age

The host chondrite NWA 8192 is of petrologic type 5/6 and, therefore, has been strongly metamorphosed with peak temperatures of ~800–950°C (e.g., Dodd 1981; Slater-Reynolds and McSween 2005). The Hf-W cooling ages of type 5 and 6 ordinary chondrites typically are between ~5 and ~12 Ma after CAI formation (Kleine et al. 2008; Archer et al. 2019; Hellmann et al. 2019). Consistent with this, the W isotopic composition of a metal separate from NWA 8192 yields a model age of 11.1 ± 2.3 Ma after CAIs, as calculated relative to the Hf-W composition of the bulk host chondrite. The model age of the metal corresponds to the time of cooling below the Hf-W closure temperature in the host chondrite during thermal metamorphism.

The three 8192-I1 subsamples are characterized by high $^{180}$Hf/$^{184}$W ratios of between ~26 and ~33 and correspondingly radiogenic $\varepsilon^{182}$W values of ~28. The elevated Hf/W of 8192-I1 is consistent with the overall depletion of siderophile elements in 8192-I1, indicating that a metallic melt was removed from the inclusion. The Hf-W data for 8192-I1 can, therefore, be used to constrain the timing of this metal–silicate fractionation by calculating a model age of Hf/W fractionation from a reservoir having chondritic Hf/W. The model age calculation assumes a single stage of Hf/W fractionation and complete metal–silicate equilibration during this event. Given that 8192-I1 was likely completely molten, combined with its occurrence in a chondritic host, these conditions are likely met.

The three 8192-I1 subsamples have variable $^{180}$Hf/$^{184}$W, but indistinguishable $\varepsilon^{182}$W. As a result, the calculated model ages for the three subsamples vary from ~0 to ~3 Ma after CAI formation (Fig. 6). As the variable $^{180}$Hf/$^{184}$W of the 8192-I1 subsamples are not accompanied by variable $\varepsilon^{182}$W, the different Hf/W ratios must have been established after effective $^{182}$Hf extinction in these samples, which given the range in $^{180}$Hf/$^{184}$W ratios among the subsamples was at ~35 Ma after CAI formation. The distinct $^{180}$Hf/$^{184}$W ratios of the three 8192-I1 subsamples were, therefore, established later than ~35 Ma after CAI formation and, thus, after the original formation of 8192-I1. It is tempting to attribute the variable Hf/W ratios of the different 8192-I1 subsamples to small variations in the abundance of metal (i.e., W concentration) and the heterogeneous distribution of Hf-rich mineral phases such as high Ca-pyroxene and phosphates. However, in this case, corresponding $\varepsilon^{182}$W variations among the three subsamples would also be expected. This is because, as shown above, closure of the Hf-W system in the host chondrite occurred at about 11 Ma. This most

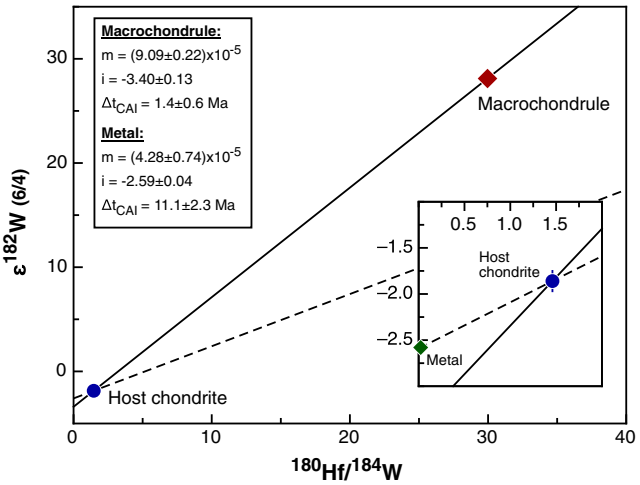


Fig. 7. Hf-W isochron diagram with two-point isochrons for Macrochondrule 8192-I1 (solid line) and metal from the host chondrite (dashed line). The W isotopic composition is reported in the ε-notation, which is the deviation of the $^{182}W/^{184}W$ of a given sample from that of an Alfa Aesar standard solution in parts per $10^4$. Note that calculation of a Hf-W model age is equivalent to constructing a two-point isochron. Inset shows magnification of the isochron near the intercept, highlighting the distinct W isotope compositions of the metal separate and the bulk chondrite NWA 8192. (Color figure can be viewed at wileyonlinelibrary.com.)

likely is also the time at which the Hf-W system in the constituent minerals of the 8192-I1 inclusion last equilibrated. However, for Hf-W closure at ~11 Ma, the different $^{180}Hf/^{184}W$ ratios of the three 8192-I1 subsamples would have evolved to an ~3 $\varepsilon^{182}W$ difference, which is not observed. Thus, the variable Hf/W ratios cannot reflect the heterogeneous distribution of metal and a Hf-rich mineral that last equilibrated during the time of parent body metamorphism. It is also unlikely that the different Hf/W ratios reflect remelting and recrystallization of the inclusion at >35 Ma after CAI formation, because such an event should have also affected the Hf-W system in the host chondrite. This is because remelting of the 8192-I1 inclusion would have required heating above the Hf-W closure temperature of ~750–950°C for type 5–6 chondrites (Kleine et al. 2008), and so would have likely resulting in W isotopic equilibration between metal and silicates. In this case, the host metal of NWA 8192 should be characterized by the same $\varepsilon^{182}W$ as the host chondrite, which again is not observed. Taking all these observations together suggests that the variable Hf/W ratios of the 8192-I1 subsamples most likely reflect the effects of mild terrestrial weathering, which resulted in a recent minor redistribution of Hf and W within the inclusion without affecting its W isotopic composition.

As noted above, the REE concentrations of 8192-I1 subsample B are indistinguishable from the weighted average concentrations of all three subsamples. The same is true for the Hf-W systematics; the weighted average of the three 8192-I1 subsamples corresponds to $^{180}Hf/^{184}W = 30.0 \pm 0.2$ and $\varepsilon^{182}W = 28.1 \pm 0.7$ (2 SD), indistinguishable from the value determined for subsample 8192-I1-B (Table 2). We, therefore, interpret this composition to be representative of the bulk 8192-I1 inclusion. The corresponding model age is $1.4 \pm 0.6$ Ma after CAI formation, which we interpret as the time of formation of 8192-I1. This model age was calculated relative to the Hf-W composition of the bulk host chondrite ($^{180}Hf/^{184}W = 1.46 \pm 0.01$, $\varepsilon^{182}W = -1.86 \pm 0.12$; Fig. 7). Identical results are obtained when the model age is calculated relative to the Hf-W composition of carbonaceous chondrites ($^{180}Hf/^{184}W = 1.35 \pm 0.03$, $\varepsilon^{182}W = -1.97 \pm 0.04$; Kruijer et al. 2014b), indicating that the model age is insensitive to the particular assumed precursor composition.

Importantly, the $1.4 \pm 0.6$ Ma model age of the 8192-I1 macrochondrule is older than the cooling age of ~11 Ma after CAIs obtained for the host metal, indicating that the macrochondrule did not isotopically re-equilibrate with the surrounding host during thermal metamorphism. This lack of re-equilibration most likely reflects the large size of the 8192-I1 inclusion. Thus, although the macrochondrule 8192-I1 derives from a strongly metamorphosed chondrite, the original formation time can still be determined from the Hf-W systematics of the bulk inclusion. To this end, it is essential that a representative bulk sample of the inclusion is analyzed, because the thermal metamorphism very likely resulted in re-equilibration of the internal Hf-W systematics of the inclusion. Consequently, unrepresentative sampling of the inclusion may result in an inaccurate model age of the inclusion. As noted above, the three subsamples of 8192-I1 combined likely provide a representative bulk composition of the inclusion, and hence, the Hf-W model age of $1.4 \pm 0.6$ Ma after CAIs can be reliably interpreted to reflect the time of the 8192-I1 inclusion.

The Hf-W model age 8192-I1 overlaps with Al-Mg ages for normal-sized chondrules from primitive ordinary chondrites, which cluster at ~2–3 Ma after CAIs (Kita et al. 2000; Rudraswami and Goswami 2007; Villeneuve et al. 2009; Pape et al. 2019). The Pb-Pb ages of some ordinary chondrite chondrules are older, and sometimes as old as CAIs (Bollard et al. 2017), but the significance of these ages and whether they date chondrule formation is debated (Kleine et al. 2018; Hellmann et al. 2019; Pape et al. 2019). Either way, the $1.4 \pm 0.6$ Ma model age of 8192-I1 overlaps

with typical formation ages of chondrules from ordinary chondrites, suggesting that both formed coevally and, as such most likely by the same process. Combined with the textural, chemical, and O isotopic evidence summarized above, this reaffirms the above conclusion that 8192-I1 is a macrochondrule.

### Implications for Chondrule Formation

The major distinctive feature of macrochondrule 8192-I1 relative to the more common ordinary chondrite chondrules is its much larger size. The final chondrule size is determined by the size of the chondrule precursor and the growth during chondrule formation (e.g., Jacquet 2014), and so the large size of macrochondrule 8192-I1 may simply reflect formation by melting of an extremely large precursor. Alternatively, 8192-I1 may have also formed from accumulated and remelted normal-sized chondrules. This may have occurred in locations with very high dust densities, where an increased number of normal-sized chondrules may have formed, so that the probability of collisions among droplets was high (e.g., Weyrauch and Bischoff 2012).

Regardless of the exact process by which 8192-I1 acquired its large size, it falls well outside the size–frequency distributions observed for normal chondrules. Average chondrule sizes increase from H to LL chondrites (e.g., Metzler 2018), most likely as a result of aerodynamic grain-size sorting (Clayton 1980; Liffman 2005). If, however, the chondrule-forming process was capable of generating cm-sized chondrules, then it is likely that the range in chondrule sizes was initially much larger than presently observed in chondrites. Perhaps, the size sorting was sufficiently efficient so that only a small range of chondrule sizes was preserved in chondrites and that larger (and smaller) chondrules than a certain threshold were preferentially lost (Metzler 2018). In this case, macrochondrules would represent rare examples of larger objects that were not lost. Another possibility is that the observed range in chondrule sizes, including the cm-sized macrochondrule studied here, represents the original size distribution of chondrules and their precursors. In this case, the low abundance of macrochondrules in chondrites would reflect their infrequent formation, perhaps because large precursors were rare.

## CONCLUSIONS

A large igneous inclusion within the equilibrated, highly metamorphosed L5/6 chondrite NWA 8192 was identified as a macrochondrule on the basis of its typical chondrule texture and chemical and O isotopic composition, all of which are similar to normal-sized chondrules. For the first time, such an individual object was successfully dated using the short-lived $^{182}$Hf-$^{182}$W system. The Hf-W model age of the macrochondrule corresponds to $1.4 \pm 0.6$ Ma after CAI formation and is interpreted to date metal–silicate separation during formation of the macrochondrule. This Hf-W age is indistinguishable from Al-Mg ages for normal-sized chondrules from primitive ordinary chondrites, which peak at ~2–3 Ma after CAIs (Kita et al. 2000; Rudraswami and Goswami 2007; Villeneuve et al. 2009; Pape et al. 2019). The Hf-W model age of metal separated from the host chondrite is ~11 Ma after CAI formation and corresponds to the time of cooling from metamorphic peak temperatures on the parent body. This age is significantly younger than the model age of the macrochondrule, indicating that the macrochondrule remained isotopically isolated from the host chondrite during thermal metamorphism on the parent body. Thus, the Hf-W system can be used to date the original formation of macrochondrules (and large igneous inclusions in general), even if they derive from highly metamorphosed host chondrites.

The contemporaneous formation of macrochondrules and normal-sized chondrules together with their similar textures, broadly similar chemical compositions, and O isotope signatures suggests that despite the large size difference, both types of chondrules formed by the same or similar processes. As such, our results imply that chondrule formation was not limited to mm-sized chondrules, but occasionally also produced chondrule sizes several orders of magnitude larger.

*Acknowledgments*—We thank Emmanuel Jacquet, Michael Weisberg, and associate editor Alex Ruzicka for their constructive reviews. This work was partially funded by the Deutsche Forschungsgemeinschaft (DFG, German Research Foundation)—Project-ID 263649064—TRR 170, and by a Laboratory Directed Research and Development grant (20-ERD-001 to T.S.K). K.M. was supported by DFG-grant ME 1115/10-1. Some of this work was conducted under the auspices of the US Department of Energy at Lawrence Livermore National Laboratory under Contract DE-AC52-07NA27344 (release number: LLNL-JRNL-656776). These sources of funding are gratefully acknowledged. The authors declare no conflict of interest. Open access funding enabled and organized by Projekt DEAL.

*Editorial Handling*—Dr. Alex Ruzicka

## REFERENCES

Archer G. J., Walker R. J., Tino J., Blackburn T., Kruijer T. S., and Hellmann J. L. 2019. Siderophile element

constraints on the thermal history of the H chondrite parent body. *Geochimica et Cosmochimica Acta* 245:556–576.

Berlin J., Jones R., Brearley A., and Spilde M. 2008. Determining bulk chemical compositions of chondrules by electron microprobe: Modal recombination versus defocused beam analyses. *Microscopy and Microanalysis* 14:110–111.

Binns R. 1967. An exceptionally large chondrule in the Parnallee meteorite. *Mineralogical Magazine and Journal of the Mineralogical Society* 36:319–324.

Bollard J., Connelly J. N., Whitehouse M. J., Pringle E. A., Bonal L., Jørgensen J. K., Nordlund Å., Moynier F., and Bizzarro M. 2017. Early formation of planetary building blocks inferred from Pb isotopic ages of chondrules. *Science Advances* 3:e1700407.

Brearley A. J. and Jones R. H. 1998. Chondritic meteorites. *Reviews in Mineralogy and Geochemistry* 36:3.1-3.398.

Bridges J. and Hutchison R. 1997. A survey of clasts and large chondrules in ordinary chondrites. *Meteoritics & Planetary Science* 32:389–394.

Budde G., Kruijer T. S., Fischer-Gödde M., Irving A. J., and Kleine T. 2015. Planetesimal differentiation revealed by the Hf–W systematics of ureilites. *Earth and Planetary Science Letters* 430:316–325.

Budde G., Kleine T., Kruijer T. S., Burkhardt C., and Metzler K. 2016. Tungsten isotopic constraints on the age and origin of chondrules. *Proceedings of the National Academy of Sciences* 113:2886–2891.

Budde G., Kruijer T. S., and Kleine T. 2018. Hf-W chronology of CR chondrites: Implications for the timescales of chondrule formation and the distribution of $^{26}$Al in the solar nebula. *Geochimica et Cosmochimica Acta* 222:284–304.

Burkhardt C., Kleine T., Bourdon B., Palme H., Zipfel J., Friedrich J. M., and Ebel D. S. 2008. Hf–W mineral isochron for Ca, Al-rich inclusions: Age of the solar system and the timing of core formation in planetesimals. *Geochimica et Cosmochimica Acta* 72:6177–6197.

Clayton D. D. 1980. Chemical and isotopic fractionation by grain size separates. *Earth and Planetary Science Letters* 47:199–210.

Clayton R. N. and Mayeda T. K. 1996. Oxygen isotope studies of achondrites. *Geochimica et Cosmochimica Acta* 60:1999–2017.

Clayton R. N. and Mayeda T. K. 1999. Oxygen isotope studies of carbonaceous chondrites. *Geochimica et Cosmochimica Acta* 63:2089–2104.

Clayton R. N., Mayeda T. K., Goswami J., and Olsen E. J. 1991. Oxygen isotope studies of ordinary chondrites. *Geochimica et Cosmochimica Acta* 55:2317–2337.

Cook D. L. and Schönbächler M. 2016. High-precision measurement of W isotopes in Fe–Ni alloy and the effects from the nuclear field shift. *Journal of Analytical Atomic Spectrometry* 31:1400–1405.

Dodd R. T. 1981. *Meteorites: A petrologic-chemical synthesis*. Cambridge: Cambridge University Press.

Ebert S. and Bischoff A. 2016. Genetic relationship between Na-rich chondrules and Ca, Al-rich inclusions?–Formation of Na-rich chondrules by melting of refractory and volatile precursors in the solar nebula. *Geochimica et Cosmochimica Acta* 177:182–204.

Ebihara M. and Honda M. 1983. Rare earth abundances in chondritic phosphates and their implications for early stage chronologies. *Earth and Planetary Science Letters* 63:433–445.

Engineering ToolBox. 2001. https://www.engineeringtoolbox.com. Accessed February 14, 2020.

Feldstein S., Jones R., and Papike J. 2001. Disequilibrium partial melting experiments on the Leedey L6 chondrite: Textural controls on melting processes. *Meteoritics & Planetary Science* 36:1421–1441.

Greenwood R., Franchi I., Gibson J., and Benedix G. 2012. Oxygen isotope variation in primitive achondrites: The influence of primordial, asteroidal and terrestrial processes. *Geochimica et Cosmochimica Acta* 94:146–163.

Griffin W. 2008. GLITTER: Data reduction software for laser ablation ICP-MS.In *Laser ablation ICP-MS in the Earth Sciences*: *Current practices and outstanding issues*, edited by Sylvester P. Vancouver: Mineralogical Society of Canada. pp. 308–311.

Grossman J. N. and Wasson J. T. 1983. The compositions of chondrules in unequilibrated chondrites an evaluation of models for the formation of chondrules and their precursor materials. In *Chondrules and their origins*, edited by King E. A. Houston, Texas: Lunar and Planetary Institute. pp. 88–121.

Hellmann J. L., Kruijer T. S., Van Orman J. A., Metzler K., and Kleine T. 2019. Hf-W chronology of ordinary chondrites. *Geochimica et Cosmochimica Acta* 258:290–309.

Jacquet E. 2014. The quasi-universality of chondrule size as a constraint for chondrule formation models. *Icarus* 232:176–186.

Jamsja N. and Ruzicka A. 2010. Shock and thermal history of Northwest Africa 4859, an annealed impact-melt breccia of LL chondrite parentage containing unusual igneous features and pentlandite. *Meteoritics & Planetary Science* 45:828–849.

Jarosewich E. 2006. Chemical analyses of meteorites at the Smithsonian Institution: An update. *Meteoritics & Planetary Science* 41:1381–1382.

Jochum K. P., Nohl U., Herwig K., Lammel E., Stoll B., and Hofmann A. W. 2005. GeoReM: A new geochemical database for reference materials and isotopic standards. *Geostandards and Geoanalytical Research* 29:333–338.

Kennedy A., Hutchison R., Hutcheon I., and Agrell S. 1992. A unique high Mn/Fe microgabbro in the Parnallee (LL3) ordinary chondrite: Nebular mixture or planetary differentiate from a previously unrecognized planetary body? *Earth and Planetary Science Letters* 113:191–205.

Kita N. T., Nagahara H., Togashi S., and Morishita Y. 2000. A short duration of chondrule formation in the solar nebula: Evidence from $^{26}$Al in Semarkona ferromagnesian chondrules. *Geochimica et Cosmochimica Acta* 64:3913–3922.

Kleine T., Münker C., Mezger K., and Palme H. 2002. Rapid accretion and early core formation on asteroids and the terrestrial planets from Hf-W chronometry. *Nature* 418:952–955.

Kleine T., Mezger K., Münker C., Palme H., and Bischoff A. 2004. $^{182}$Hf-$^{182}$W isotope systematics of chondrites, eucrites, and Martian meteorites: Chronology of core formation and early mantle differentiation in Vesta and Mars. *Geochimica et Cosmochimica Acta* 68:2935–2946.

Kleine T., Touboul M., Van Orman J. A., Bourdon B., Maden C., Mezger K., and Halliday A. N. 2008. Hf–W thermochronometry: Closure temperature and constraints on the accretion and cooling history of the H chondrite

parent body. *Earth and Planetary Science Letters* 270:106–118.

Kleine T., Hans U., Irving A. J., and Bourdon B. 2012. Chronology of the angrite parent body and implications for core formation in protoplanets. *Geochimica et Cosmochimica Acta* 84:186–203.

Kleine T., Budde G., Hellmann J., Kruijer T. S., and Burkhardt C. 2018. Tungsten isotopes and the origin of chondrules and chondrites. In *Chondrules: Records of protoplanetary disk processes*, edited by Russell S. S., Connolly H. C., and Krot A. N. Cambridge: Cambridge University Press. pp. 276–299.

Kleine T. and Walker R. J. 2017. Tungsten isotopes in planets. *Annual Review of Earth and Planetary Sciences* 45:389–417.

Kruijer T. S., Sprung P., Kleine T., Leya I., Burkhardt C., and Wieler R. 2012. Hf–W chronometry of core formation in planetesimals inferred from weakly irradiated iron meteorites. *Geochimica et Cosmochimica Acta* 99:287–304.

Kruijer T., Touboul M., Fischer-Gödde M., Bermingham K., Walker R., and Kleine T. 2014a. Protracted core formation and rapid accretion of protoplanets. *Science* 344:1150–1154.

Kruijer T. S., Kleine T., Fischer-Gödde M., Burkhardt C., and Wieler R. 2014b. Nucleosynthetic W isotope anomalies and the Hf–W chronometry of Ca–Al-rich inclusions. *Earth and Planetary Science Letters* 403:317–327.

Liffman K. 2005. Chondrule and metal grain size sorting from jet flows. *Meteoritics & Planetary Science* 40:123–138.

Lodders K. 2003. Solar system abundances and condensation temperatures of the elements. *The Astrophysical Journal* 591:1220–1247.

McSween H. Y. and Huss G. R. 2010. *Cosmochemistry*. Cambridge: Cambridge University Press.

Meteoritical Bulletin Database. 2020. https://www.lpi.usra.edu/meteor/. Accessed February 17, 2020.

Metzler K. 2018. From 2D to 3D chondrule size data: Some empirical ground truths. *Meteoritics & Planetary Science* 53:1489–1499.

Metzler K. and Pack A. 2016. Chemistry and oxygen isotopic composition of cluster chondrite clasts and their components in LL 3 chondrites. *Meteoritics & Planetary Science* 51:276–302.

Metzler K., Bischoff A., Greenwood R. C., Palme H., Gellissen M., Hopp J., Franchi I. A., and Trieloff M. 2011. The L3–6 chondritic regolith breccia Northwest Africa (NWA) 869:(I) Petrology, chemistry, oxygen isotopes, and Ar-Ar age determinations. *Meteoritics & Planetary Science* 46:652–680.

Newton J., Franchi I., and Pillinger C. 2000. The oxygen-isotopic record in enstatite meteorites. *Meteoritics & Planetary Science* 35:689–698.

Pack A., Tanaka R., Hering M., Sengupta S., Peters S., and Nakamura E. 2016. The oxygen isotope composition of San Carlos olivine on the VSMOW2-SLAP2 scale. *Rapid Communications in Mass Spectrometry* 30:1495–1504.

Pape J., Mezger K., Bouvier A.-S., and Baumgartner L. P. 2019. Time and duration of chondrule formation: Constraints from $^{26}$Al-$^{26}$Mg ages of individual chondrules. *Geochimica et Cosmochimica Acta* 244:416–436.

Pourmand A., Dauphas N., and Ireland T. J. 2012. A novel extraction chromatography and MC-ICP-MS technique for rapid analysis of REE, Sc and Y: Revising CI-chondrite and Post-Archean Australian Shale (PAAS) abundances. *Chemical Geology* 291:38–54.

Prinz M., Weisberg M., and Nehru C. 1988. Gunlock, a new Type 3 ordinary chondrite with a golfball-sized chondrule. *Meteoritics* 23:297.

Rudraswami N. G. and Goswami J. N. 2007. $^{26}$Al in chondrules from unequilibrated L chondrites: Onset and duration of chondrule formation in the early solar system. *Earth and Planetary Science Letters* 257:231–244.

Ruzicka A., Snyder G. A., and Taylor L. A. 1998. Mega-chondrules and large, igneous-textured clasts in Julesberg (L3) and other ordinary chondrites: Vapor-fractionation, shock-melting, and chondrule formation. *Geochimica et Cosmochimica Acta* 62:1419–1442.

Ruzicka A., Hutson M., Floss C., and Hildebrand A. 2012. Large silica-rich igneous-textured inclusions in the Buzzard Coulee chondrite: Condensates, differentiates, or impact melts? *Meteoritics & Planetary Science* 47:1809–1829.

Ruzicka A., Snyder G. A., and Taylor L. A. 2000. Geochemical and isotopic evidence bearing on the origin of large igneous-textured inclusions in ordinary chondrites. *Antarctic Meteorite Research* 13:19–38.

Ruzicka A. M., Greenwood R. C., Armstrong K., Schepker K. L., and Franchi I. A. 2019. Petrology and oxygen isotopic composition of large igneous inclusions in ordinary chondrites: Early solar system igneous processes and oxygen reservoirs. *Geochimica et Cosmochimica Acta* 266:497–528.

Sack R. O., Ghiorso M. S., Wang M. S., and Lipschutz M. E. 1994. Igneous inclusions from ordinary chondrites: High temperature cumulates and a shock melt. *Journal of Geophysical Research: Planets* 99:26029–26044.

Slater-Reynolds V. and McSween H. Y. 2005. Peak metamorphic temperatures in type 6 ordinary chondrites: An evaluation of pyroxene and plagioclase geothermometry. *Meteoritics & Planetary Science* 40:745–754.

Touboul M., Sprung P., Aciego S. M., Bourdon B., and Kleine T. 2015. Hf–W chronology of the eucrite parent body. *Geochimica et Cosmochimica Acta* 156:106–121.

Van Achterbergh E., Ryan C.G., Jackson S. E., and Griffin W. L. 2001. Data reduction software for LA-ICP-MS: Appendix. In *Laser ablation-ICP-mass spectrometry in the Earth sciences: Principles and applications*, edited by Sylvester P. Ottawa: Mineralogical Association of Canada. pp. 239–243.

Villeneuve J., Chaussidon M., and Libourel G. 2009. Homogeneous distribution of $^{26}$Al in the solar system from the Mg isotopic composition of chondrules. *Science* 325:985–988.

Ward D., Bischoff A., Roszjar J., Berndt J., and Whitehouse M. J. 2017. Trace element inventory of meteoritic Ca-phosphates. *American Mineralogist: Journal of Earth and Planetary Materials* 102:1856–1880.

Weisberg M., Prinz M., and Nehru C. 1988. Macrochondrules in ordinary chondrites: Constraints on chondrule forming processes. *Meteoritics* 23:309.

Weyrauch M. and Bischoff A. 2012. Macrochondrules in chondrites—Formation by melting of mega-sized dust aggregates and/or by rapid collisions at high temperatures? *Meteoritics & Planetary Science* 47:2237–2250.

Wiechert U., Halliday A., Palme H., and Rumble D. 2004. Oxygen isotope evidence for rapid mixing of the HED meteorite parent body. *Earth and Planetary Science Letters* 221:373–382.

Willbold M., Elliott T., and Moorbath S. 2011. The tungsten isotopic composition of the Earth's mantle before the terminal bombardment. *Nature* 477:195–199.

Wlotzka F. 1993. A weathering scale for the ordinary chondrites. *Meteoritics* 28:460.